Microscopy Research and Technique, 1–16. https://doi.org/10.1002/jemt. 24394

The effect of ultrafine WO_3 nanoparticles on the organization of thylakoids enriched in photosystem II and energy transfer in photosystem II complexes

S. Krysiak[1] | M. Gotić[2] | E. Madej[3] | A. C. Moreno Maldonado[4] | G. F. Goya[4] | N. Spiridis[3] | K. Burda[1]

[1]Faculty of Physics and Applied Computer Science, AGH – University of Krakow, Krakow, Poland

[2]Division of Materials Physics, Ruđer Bošković Institute, Zagreb, Croatia

[3]Jerzy Haber Institute of Catalysis and Surface Chemistry, Polish Academy of Sciences, Krakow, Poland

[4]Condensed Matter Physics Department and Instituto de Nanociencia y Materiales de Aragón, Universidad de Zaragoza, Zaragoza, Spain

Correspondence
K. Burda, Faculty of Physics and Applied Computer Science, AGH – University of Krakow, al. Mickiewicza 30, 30-059 Krakow, Poland.
Email: kvetoslava.burda@fis.agh.edu.pl

Funding information
EU Project, Grant/Award Number: POWR.03.02.00-00-I004/16

Review Editor: Prof. Jose Luis Toca-Herrera

Abstract

In this work, a new approach to construct self-assembled hybrid systems based on natural PSII-enriched thylakoid membranes (PSII BBY) is demonstrated. Superfine m-WO_3 NPs (≈1–2 nm) are introduced into PSII BBY. Transmission electron microscopy (TEM) measurements showed that even the highest concentrations of NPs used did not degrade the PSII BBY membranes. Using atomic force microscopy (AFM), it is shown that the organization of PSII BBY depends strongly on the concentration of NPs applied. This proved that the superfine NPs can easily penetrate the thylakoid membrane and interact with its components. These changes are also related to the modified energy transfer between the external light-harvesting antennas and the PSII reaction center, shown by absorption and fluorescence experiments. The biohybrid system shows stability at pH 6.5, the native operating environment of PSII, so a high rate of O_2 evolution is expected. In addition, the light-induced water-splitting process can be further stimulated by the direct interaction of superfine WO_3 NPs with the donor and acceptor sides of PSII. The water-splitting activity and stability of this colloidal system are under investigation.

Research Highlights

- The phenomenon of the self-organization of a biohybrid system composed of thylakoid membranes enriched in photosystem II and superfine WO_3 nanoparticles is studied using AFM and TEM.
- A strong dependence of the organization of PSII complexes within PSII BBY membranes on the concentration of NPs applied is observed.
- This observation turns out to be crucial to understand the complexity of the mechanism of the action of WO_3 NPs on modifications of energy transfer from external antenna complexes to the PSII reaction center.

KEYWORDS
absorption and fluorescence spectroscopy, atomic force microscopy, photosystem II, thylakoids, WO_3 nanoparticles

Abbreviations: AFM, atomic force microscopy; Chl, chlorophyll; CP24, CP26 and CP29, minor light-harvesting antennas; CP43 and CP47, inner light-harvesting antennas; cyt. b_{559}, cytochrome b_{559}; DLS, dynamic light scattering method.; LHC II, light-harvesting complex II (major component of the outer light-harvesting antennas); m-WO_3, monoclinic tungsten trioxide; NP, nanoparticle; NPQ, non-photochemical quenching; OEC, oxygen-evolving complex; P680, special pair of Chl *a*; Pheo, pheophytin; PQ, plastoquinone; PQH_2, plastoquinol; PSII BBY, thylakoids enriched in PSII; PSII, photosystem II; Q_A, PSII primary quinone electron acceptor; Q_B, PSII secondary quinone electron acceptor; RC, reaction center; TEM, transmission electron microscopy; WOC, water-oxidizing complex; XPS, X-ray photoelectron spectroscopy; Y_D, tyrosine residue of D2 protein; Y_Z, tyrosine residue of D1 protein.

1 | INTRODUCTION

It is estimated that about 50% of the wavelength range of sunlight reaching the Earth's surface is used by photosynthetic organisms. The high efficiency of light absorption and charge separation in reaction centers (RCs) makes photosynthetic systems very attractive for their application in biohybrid solar cells/reactors (Gust et al., 2009; Liu & van Iersel, 2021; McCree, 1972; Sager et al., 1988; Wasilewski, 2009; Xu et al., 2017). Photosystem II (PSII) (Figure 1) has the most efficient light transformative capability on Earth (energy efficiency for absorbed photons with respect to charge separation is ~84%) (McConnell et al., 2010). Moreover, it can drive the solar water splitting process due to its extremely high oxidative power (highest among natural photosynthetic systems: 1.8 V at each photochemical step) and the presence of a Mn_4CaO_5 cluster (called an oxygen-evolving complex – OEC or a water-oxidizing complex – WOC) located on its donor side (Figure 1). Under environmental conditions, PSII is able to use 75% of the energy absorbed by its reaction center to split water and has 1.2 V of its oxidizing power to do so at each oxidation step (Pecoraro et al., 1998). For this reason, many research groups investigating renewable energy sources and fuel cells that can use water as an electron and proton donor are interested in the bionics of photosystem II.

The challenge lies in designing "super-catalysts" for the anodic reaction to increase the kinetics of O_2 evolution and avoid the formation of other chemicals on the anode surface (Madey & Yates, 1968). The disadvantage of metal oxide anodes (especially TiO_2, ZnO or WO_3) is the high overpotential, which has a direct effect on the conversion efficiency (Grätzel, 2001). Current research in photocatalytic water splitting focuses on the design of photoanodes characterized by (i) efficient charge separation, (ii) fast charge transfer kinetics, (iii) activation over a wide range of the visible light spectrum, and (iv) stability under ambient conditions. Various attempts are made to modify known, existing solid-state systems by doping, functionalizing their surfaces, using dyes, depositing noble metals and combining them into cooperative heterostructures according to the scheme Z (reviews: [Jafari et al., 2016; Lee et al., 2019; Li & Tsang, 2020; Sumathi et al., 2019; Wang et al., 2020; Yamanoi et al., 2021]).

The combination of inorganic semiconductors/metals and natural photosynthetic isolated antenna complexes and even more complex protein-lipid-pigment systems, such as entire photosystems, in biohybrid systems is opening a promising area for new research on water photocatalysis (Badura et al., 2006; Grimme et al., 2008; Ihara et al., 2006; Iwuchukwu et al., 2010; Kato et al., 2013; Kawahara et al., 2020; Li et al., 2016; Miyachi et al., 2017; Nagakawa et al., 2019; Riedel et al., 2019; Tahara et al., 2017; Terasaki et al., 2008; Tian et al., 2021; Utschig et al., 2011; Vittadello et al., 2010; Voloshin et al., 2022; Yehezkeli et al., 2012; Yehezkeli et al., 2014; Zhang & Reisner, 2020). These biohybrids are expected to be environmentally safe and use solar energy with near 100% efficiency. It seems evident that a new generation of systems capable of oxidizing water with the efficiency of evolutionarily selected photosystems should be based on natural PSII and n-semiconductors, which are known for their high stability in aqueous environments over a wide pH range. Most efficient semiconductors absorb below 500 nm, but when combined with PSII and/or external photosynthetic antennas, biohybrid anodes have no such limitations on absorbed sunlight (for review, see: [Gonçalves Silva et al., 2022; Liu et al., 2018; Pang et al., 2018; Voloshin et al., 2022; Zhang & Reisner, 2020]). Previous studies have been limited to photosynthetic systems deposited on non-functionalized or functionalized surfaces, which limited the density of photosystems that could be attached to and in direct contact with flat electrodes and forced the orientation and packing pattern of the photosystems. For a variety of systems, substrate porosity have been shown to increase the contact area with biological molecules and significantly enhance the activity of engineered biohybrids (Hardee & Bard, 1977; Huang et al., 2015; Kato et al., 2012; Pang et al., 2018; Tian et al., 2021; Wang et al., 2015; Zhang & Reisner, 2020). Biohybrids formed from photosystem I and fine Pt nanoparticles are an example of another approach to producing self-organizing systems that exhibit high photocatalytic efficiency, in this case in the production of H_2 (Utschig et al., 2023).

In this work, an approach is presented in which the biohybrid system that can act as a photoanode is a colloidal system formed from superfine nanoparticles suspended with PSII-enriched photosynthetic membranes, called thylakoids (PSII BBY) in an aqueous buffer. This allows the system to self-assemble and the NPs to be in full contact with the photosynthetic membrane and its photoactive protein–dye complexes (i.e., PSII reaction center and light-harvesting complexes). WO_3 NPs were chosen due to their ability to oxidize water in the presence of an electron acceptor, which was recognized as early as the 1960's (Krasnovskii & Brin, 1962). However, due to their large energy gap between the valence and conducting bands (~2.6–3 eV), their quantum yield in the production of O_2 from water is less than 3% (Krasnovskii & Brin, 1962). It is anticipated that WO_3 NPs may oxidize the donor side and reduce the acceptor side of PSII taking into account the energies of its valence and conducting bands (Darwent & Mills, 1982; Grätzel, 2001; Zhao et al., 2014) and redox potential values of PSII redox active components (De Causmsecker et al., 2019; Ishikita & Knapp, 2006; Kato et al., 2009; Mandal et al., 2020; Rutherford et al., 1981; Shibamoto et al., 2009; Vass & Styring, 1991). Thus, these colloidal biohybrids are expected to exhibit new properties desirable for robust photocatalysts for water splitting that do not require external electron acceptors. This aspect is being studied independently. Here, the main objective is to study how the organization

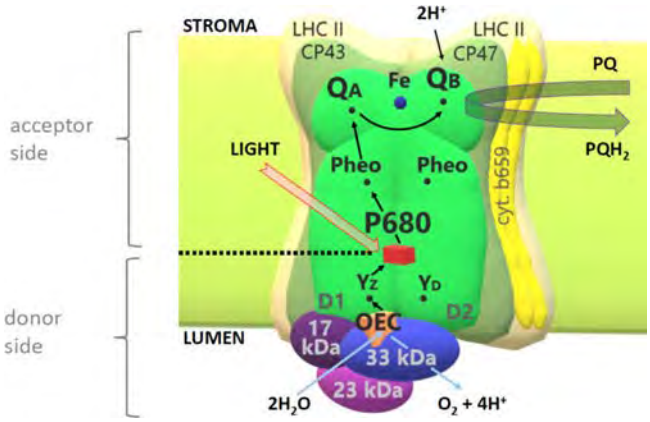

FIGURE 1 Simplified scheme of higher plant PSII complex organization in thylakoid membranes. It omits the small internal proteins with the exception of cytochrome b_{559}. (Ferreira et al., 2004; Umena et al., 2011). The lumen and stroma are the inner and outer sides of the thylakoids, respectively. The reaction core of PSII is formed by a heterodimeric protein complex consisting of the polypeptides D1 and D2, which contain redox cofactors active in the photosynthetic electron transport chain. D1 and D2 proteins are associated with two inner antenna subunits, CP43 and CP47. Three outer proteins of about 17, 23 and 33 kDa on the donor side of PSII protect the oxygen-evolving complex (OEC), containing four Mn ions, one Ca ion, and five oxygen atoms forming the Mn_4CaO_5 cluster (Ferreira et al., 2004; Umena et al., 2011). PSII catalyzes the light-induced transfer of electrons from water to plastoquinone (Kern & Renger, 2007). The absorption of light by a chlorophyll dimer P680 (a specific pair of Chls *a*) is followed by charge separation. Electron transfer occurs from the excited P680* to a primary electron acceptor, pheophytin (Pheo). Primary charge separation is stabilized when $P680^{\bullet+}$ and $Pheo^{\bullet-}$ react with other molecules on the reducing and oxidizing sides of PSII, respectively. The Pheo anion transfers an electron to a secondary electron acceptor, a tightly bound plastoquinone molecule Q_A, producing $Q_A^{\bullet-}$. Reduced Q_A transfers the electron to a second plastoquinone molecule at the Q_B site. This electron transfer is aided by the non-heme iron located between the Q_A and Q_B sites (Burda, 2007). A plastoquinone (PQ) molecule at the Q_B site accepts two electrons and two protons from the stroma side of the thylakoids. The reduced PQH_2 is then replaced by an oxidized plastoquinone from the membrane pool. Simultaneously, $P680^{\bullet+}$oxidizes a manganese complex. This electron transfer is mediated by a tyrosine residue of protein D1, Y_Z. Only after the accumulation of four positive charges in the OEC, O_2 is released from water: $2H_2O \rightarrow 4e^- + 4H^+ + O_2$ (Joliot et al., 1969; Kok et al., 1970). Thus, the donor side of PSII operates as a four-cycle and the acceptor side as a two-cycle.

of PSII-enriched photosynthetic membranes changes under the influence of different concentrations of superfine WO_3 NPs, and how these changes affect energy transfer to reaction centers. The stability of PSII BBY membranes treated with NPs was tested using the transmission electron microscope, TEM. Atomic force microscopy (AFM), is a unique tool for studying biosystems in their native aqueous environment and was therefore used to follow changes in thylakoid membrane organization resulting from interactions with WO_3 NPs. Absorption and fluorescence spectroscopy were used to study the effects of tungsten oxide nanoparticles on the absorption properties and energy transfer performance of BBY PSII.

2 | MATERIALS AND METHODS

Photosynthetic membranes, thylakoids, enriched in photosystem II (PSII BBY) were isolated from *Spinacia oleracea*, purchased from the local market, according to the procedure described in (Berthold et al., 1981) omitting the second Tris-washing. The freshly isolated thylakoids were suspended in the Hepes II buffer (15 mM NaCl, 5 mM $MgCl_2$, 20 mM Hepes, 400 mM sucrose), frozen in liquid nitrogen, and stored at −80°C. Before measurements, they were thawed out on ice and kept at 4°C in the darkness.

Monoclinic WO_3 nanoparticles (m-WO_3 NPs) were obtained from tungsten trioxide hydrate. A complete synthesis procedure is given in (Gotic et al., 2000), sample W3600. Briefly, 300 mL of 0.7 M HCl was added to 100 mL of the 1.0 M $Na_2WO_4{\cdot}2H_2O$ solution until the final pH of the clear solution was 1.4. The obtained solution was autoclaved at 60°C for 48 h, then isolated by centrifugation, and then dried in a Petri dish at 60°C. This white powder sample ($WO_3{\cdot}0.33H_2O$) was thermally treated at 600°C to obtain yellowish m-WO_3 nanoparticles.

The atomic composition and the chemical state of WO_3 NPs was verified using x-ray photoelectron spectroscopy (XPS). Measurements were performed with a hemispherical analyzer (SES R4000, Gamma-data Scienta, pass energy 100 eV). Core excitations were generated using an unmonochromatized Al Kα x-ray source (1486 eV, 12 kV, 15 mA) without a charge neutralizer. The energy resolution of the system, measured as full width at half maximum Ag $3d_{5/2}$ excitation line, was 0.9 eV. The spectra were calibrated for a carbon C 1s excitation at binding energy of 285 eV.

WO_3 NPs were suspended in the Hepes I buffer (15 mM NaCl, 5 mM $MgCl_2$, 20 mM Hepes) at the initial 2 mg/mL concentration. Before each experiment, they were sonicated in a water bath for 20 min at 20°C. Their size distribution in the aqueous environment was checked using the dynamic light scattering method (DLS). The applied analyzer Zetasizer Nano ZS (Malvern Panalytical Instruments) can detect NPs sizes from 0.3 nm to 10 μm. The measurements were carried out at 25°C. The wavelength of the laser was 633 nm, and the angle at which the scattered light was measured was 173°.

Suspensions of PSII BBY containing 51.2 μg of chlorophyll were treated with different concentrations of WO_3 NPs varied from 0.00512 μg/mL up to 51.2 μg/mL. Regardless of the type of measurement, the number of NPs was adjusted to the weight ratios of WO_3 NPs to chlorophyll from 0.0001 to 1.

2.1 | Imaging

Transmission electron microscopy (TEM) was applied to visualize possible changes in the structures of PSII BBY resulting from the action of WO_3 NPs. The thylakoid membranes enriched in PSII (PSII BBY)

were fixed by immersing them in a solution of 4% glutaraldehyde in 0.2 M sodium cacodylate for 2 h at 4°C. After fixation, the membranes were centrifuged at 180 G for 10 min, and then rinsed with 2 mL of a 2% glutaraldehyde solution in 0.1 M sodium cacodylate buffer. Then they were centrifuged and washed three times with 0.1 M sodium cacodylate buffer. Ultrathin 60–80 nm sections were obtained by ultramicrotomy of fixed samples embedded in epoxy resin. These sections were then mounted on a formvar and carbon double film supported on copper grid with a mesh structure for microscopic analysis. To obtain high contrast samples, osmium tetraoxide (2%) was used. The measurements were performed by TEM using a Tecnai T20 (ThermoFisher Scientific) with an image resolution of 0.24 nm at 200 kV.

Atomic force microscopy was used to monitor the organization of PSII BBY untreated and treated with different concentrations of m-WO_3 NPs. Topography was examined in a contact mode in a liquid cell with AFM 5500 (Agilent, USA). Silicon nitride probes with a soft triangular cantilever (Veeco, model MLCT) with a nominal spring constant value of 0.01 N/m were used. A glass slide used as a substrate was kept for 24 h in ethanol. Then it was flushed with distilled water and dried by evaporation in the air at 20°C. A sample drop was put on the glass surface and kept for 12 h in the air at 20°C in the dark. Then it was flushed with the Hepes I buffer and finally covered with it. Images were collected at 20°C with the resolution 515 × 512 points/line. The scan speed was 0.35 line s^{-1}. The scanning speed was chosen to optimize the measuring conditions and to obtain reproducible images for each sample at the same resolution. All samples were prepared in the same way.

2.2 | Absorption and fluorescence measurements

The influence of WO_3 NPs on the light-harvesting by PSII BBY was monitored by absorption and fluorescence measurements using UV–VIS Spectrophotometer Varian Cary 50 Bio (USA) and Cary Eclipse Fluorescence Spectrometer Agilent (USA), respectively. Emission fluorescence experiments were conducted in the wavelength range from 600 to 850 nm, under excitation radiation varying from 375 to 495 nm in 5 nm increments, at room temperature.

3 | RESULTS

Figure 2 shows the XPS spectrum obtained for WO_3 NPs. The tungsten line shows a W 4f doublet at energies of 36.1 eV (W $4f_{7/2}$) and 38.2 eV (W $4f_{5/2}$). The spin-orbit splitting of the W 4f line is 2.1 eV. These results confirm that the nanoparticles are composed of WO_3 and tungsten is in the 6^+ oxidation state (Cai et al., 2015; Keereeta et al., 2015).

Figure 3a shows an example TEM image of polycrystalline m-WO_3 NPs structures observed after sonication. The results of DLS measurements of sonicated NPs suspended in the Hepes I buffer

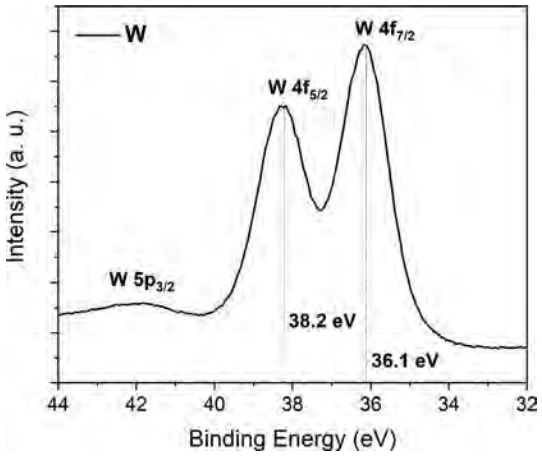

FIGURE 2 High resolution x-ray photoelectron spectrum of W 4f core level of m-WO_3 NPs.

(Figure 3b) showed the presence of ultrafine WO_3 NPs with sizes of 0.68 ± 0.10, 1.30 ± 0.30, and 1.78 ± 0.31 nm. They accounted for 70% to 100% of the volume fraction in samples containing the highest nanoparticle concentrations tested. The fractions of larger nanoparticles and their sizes depended mainly on the time since sonication. However, larger crystalline structures were also present in the samples. In the DLS measurements, the larger nanoparticles observed had a size of about 80 ± 9 nm or from about 130 ± 50 to 530 ± 150 nm, having a large dispersion. Theoretical calculations show that in monoclinic WO_3 crystals the W–O bond distance is about 1.8 Å, and the W–W distance between two corner [WO_6]-octahedra about 3.8 Å (Juelsholt et al., 2021). Theoretical data usually yield parameters slightly overestimated than the experimental data, which for W–O distances vary between 1.72 and 2.15 Å (Loopstra & Boldrini, 1966). The experimentally determined size of WO_3 elemental cell is about 7.3 Å × 7.53 Å × 7.68 Å (Tanisaki, 1960). Thus, the smallest WO_3 nanostructures observed correspond to a cell containing eight molecules of WO_3. A similar result is obtained by assuming that the tungsten trioxide nanoparticles are spherical with a diameter of about 0.7 nm (a volume of ∼0.179 nm^3), the average radius of a WO_3 particle is about 1.8 Å (a volume of ∼0.024 nm^3) and the distance of the W-O-W bond is about 3.6 Å. Similarly, it can be estimated that the nanoparticles with diameters of about 1.3 nm (a volume of ∼1.150 nm^3) and 1.78 nm (a volume of ∼2.953 nm^3) contain about 48 and 123 WO_3 particles, respectively. Note that these numbers are of the same order as 4^3 and 5^3, which would result from a dimensional analysis.

3.1 | Imaging

The nanoparticles ranging in size from 0.7 to 3 nm can easily penetrate PSII BBY membranes. To see how different concentrations of m-WO_3 NPs can affect the organization of PSII BBY, AFM topography measurements were performed.

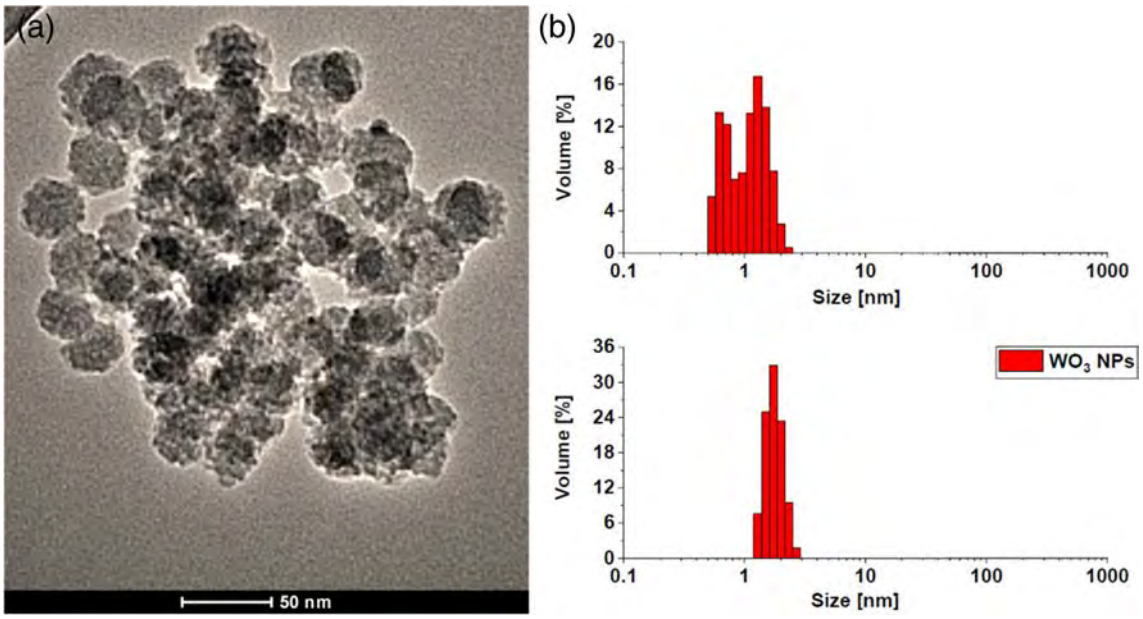

FIGURE 3 (a) Transmission electron microscopy images of example structures of m-WO_3 NPs formed after sonication. (b) Results of DLS measurements of WO_3 NPs immediately after sonication. Example volume distributions for nanoparticles with concentrations corresponding to the ratio 0.1 and 1 μg NPs/μg Chl are shown in the upper and lower graphs, respectively. WO_3 NPs were suspended in the Hepes I buffer. The Hepes I buffer gave no signal in DLS measurements. In the upper graph, the contribution of the NPs with an average size of about 0.7 and 1.3 nm is about 35% and 65%, respectively.

Figure 4a,b show example AFM images of PSII BBY untreated and treated with WO_3 NPs at a weight ratio of 1 μg NP/μg Chl. Visible protrusions about 0.3 nm high (Figure 4a,b) are the external proteins protecting OEC (Mn_4CaO_5) on the donor side of PSII (see Figure 1). The heights of the protrusions and the heights of the concavities they form, estimated from AFM measurements carried out in an aqueous environment using the tapping mode, were about 2 and 1 nm, respectively (Stoichev et al., 2015; Sznee et al., 2011), while Cryo-EM allowed setting the upper limit of the protruding structure height at about 5 nm (Nield et al., 2000). The root mean square (RMS) roughness obtained for the PSII BBY control and NPs-treated samples (Table 1) show that the observed protrusions are similar in all cases, but their heights are lower than those found in other experiments. This is due to the fact that the AFM measurements were performed in a liquid environment in the contact mode and to the tip used. Thus, the protruding parts indicate the distribution of PSII in the membranes studied. The results of the analysis of the distribution of PSII in the control sample and in samples containing strictly defined concentrations of NPs are shown in Figure 4c. Parameters of the theoretical fits using the modified Gaussian function are collected in Table 1. The deviations from the Gaussian shape are modeled by making the standard deviation linearly dependent on the argument: $\sigma = \sigma_0(1 + \varepsilon(x - x_0))$. This is an effective description that can be applied only in a specific range of x, that is, when $\varepsilon \leq \frac{1}{3}$ since σ has to be positive. This approach allowed us to simplify the description of the observed asymmetry of PSII separations.

The estimated average PSII spacing was ~7.1 nm in the control sample for the tungsten oxide measurement series and varied with increasing concentrations of added WO_3 NPs. The smallest distance of ~4.8 nm was observed for a sample containing 0.001 μg NPs/μg Chl. At higher concentrations of the WO_3 NPs tested, the average separation between PSII complexes increased and was greater than that found for the control sample. The largest distance between the PSII complexes was observed to be ~9.2 nm for a weight ratio of 0.1 μg NPs/μg Chl. The parameter ε, which is related to the asymmetry of the distribution, has the highest values for the two lowest concentrations of NPs applied. It decreases as the concentration of nanoparticles increases. For the two highest NPs concentrations used, the PSII distance distributions are close to a Gaussian function.

At the same time, it is noteworthy that even at the highest concentrations of WO_3 NPs used, fragments of the PSII-enriched thylakoids do not disintegrate (Figure 5). Due to the need for a contrast agent, it is not possible to indicate the fine WO_3 NPs in thylakoid membranes, but this was possible on the observed isolated structures of LHCII-associated and LHCII-free PSII complexes, $C_2S_2M_2$ (its size estimated on the high-resolution cryo-EM map: 19.5 nm × 31.0 nm × 12.2 nm: width × length × height) (van Bezouwen et al., 2017) and C_2 (about 10 nm × 19 nm × 11 nm: width × length × height) (Boekema et al., 1995; Haniewicz et al., 2015; Nield & Barber, 2006; Umena et al., 2011), respectively, see inset in Figure 5d.

3.2 | Absorption and fluorescence measurements

Absorption spectra of the control sample and PSII BBY treated with different concentrations of WO_3 NPs are presented in Figure 6a.

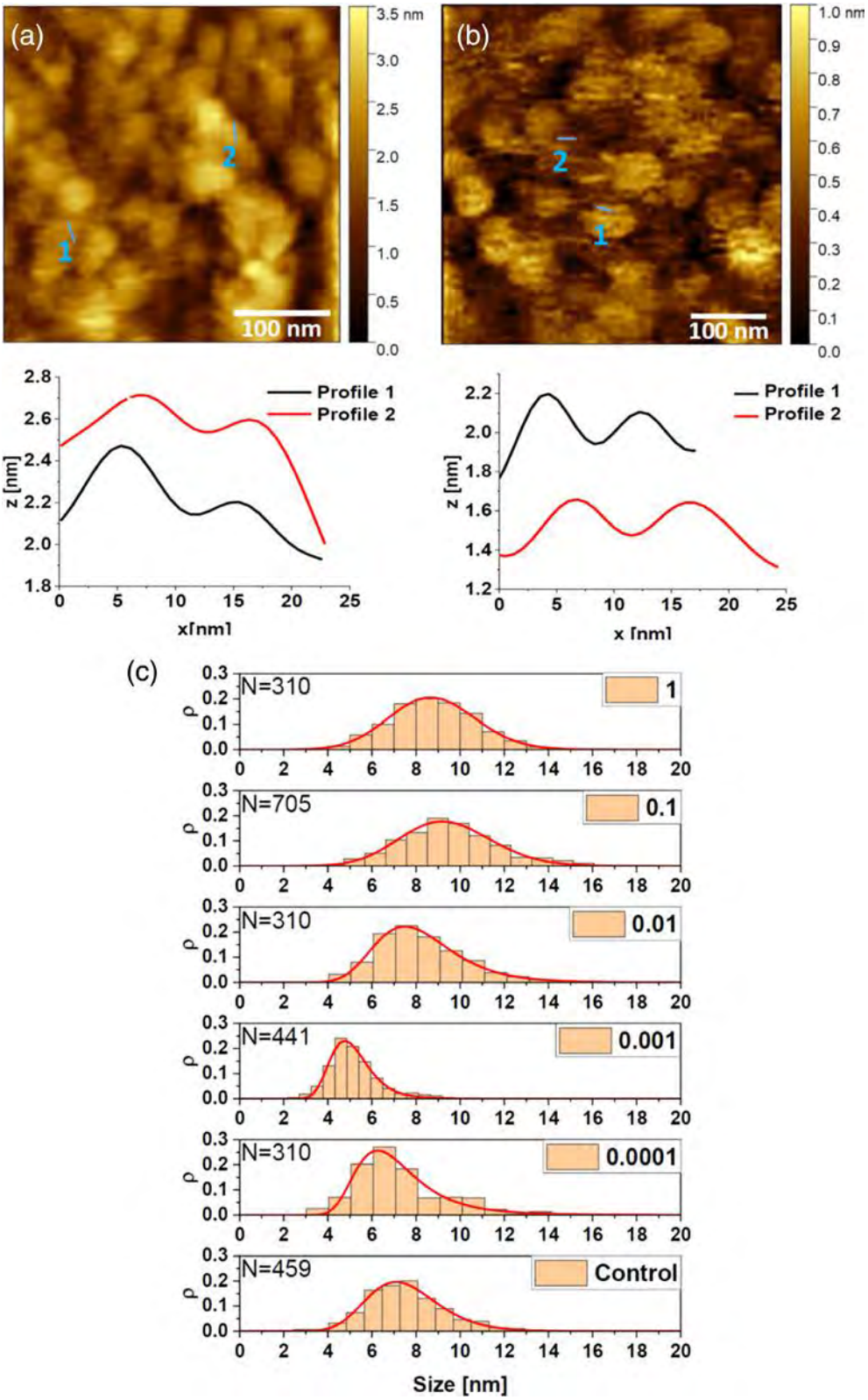

FIGURE 4 Example atomic force microscopy image of PSII BBY untreated (a) and treated with m-WO_3 NPs at a weight ratio of 1 μg NPs/μg Chl. (b). Cross sections through the protrusions marked on the topographies are shown below the images (profiles 1 and 2). (c) Distribution of PSII in the control sample of PSII BBY and samples containing indicated concentrations of NPs. The lines are theoretical fits using a modified Gaussian function (as described in the text). The fitted parameters are summarized in Table 1. Measurements done in a contact mode using a liquid cell, in the Hepes I buffer.

They show that the absorption is enhanced for samples containing 0.01 and 0.1 μg NPs/μg Chl. All spectra show two absorption bands for pigments present in both the PSII and LHCII complexes. The first band is visible in the range from 300 to about 525 nm. It is characteristic of Chls *a* and *b* (Soret B – bands) and carotenoids (Lichtenthaler & Buschmann, 2001). The second band for wavelengths >560 nm comes from Chl *b* and Chl *a* (Q bands; Q_y bands at λ > 600 nm): (i) Chl *a* and *b* from LHCII and the minor antennas with maxima at ~670–678 and ~640–654 nm, respectively, (ii) Chl *a* from the PSII complex with maxima at ~668 nm (accessory Chl *a* in the PSII

TABLE 1 Parameters of the theoretical fits of the distribution of PSII in the PSII BBY untreated and treated with WO_3 NPs (AFM experiments) using modified Gaussian function $y = C * \exp\left(\frac{-(x-x_0)^2}{2\sigma^2}\right)$, where C is the amplitude, x_0 is the abscissa of the maximum value, σ is the standard deviation linearly dependent on the argument: $\sigma = \sigma_0(1 + \varepsilon(x - x_0))$. The last row contains the root mean square (RMS) roughness obtained for the PSII BBY control and NPs-treated samples.

	Concentration (μg NPs/μg Chl)					
Parameters	**0 control**	**0.0001**	**0.001**	**0.01**	**0.1**	**1**
C	0.24	0.26	0.43	0.22	0.19	0.21
x_0 (nm)	7.09	6.26	4.77	7.49	9.19	8.66
σ_0 (nm)	1.57	1.32	0.83	1.69	2.05	1.95
ε (nm^{-1})	0.06	0.14	0.16	0.08	0.02	0.01
RMS (nm)	0.26	0.23	0.18	0.26	0.24	0.26

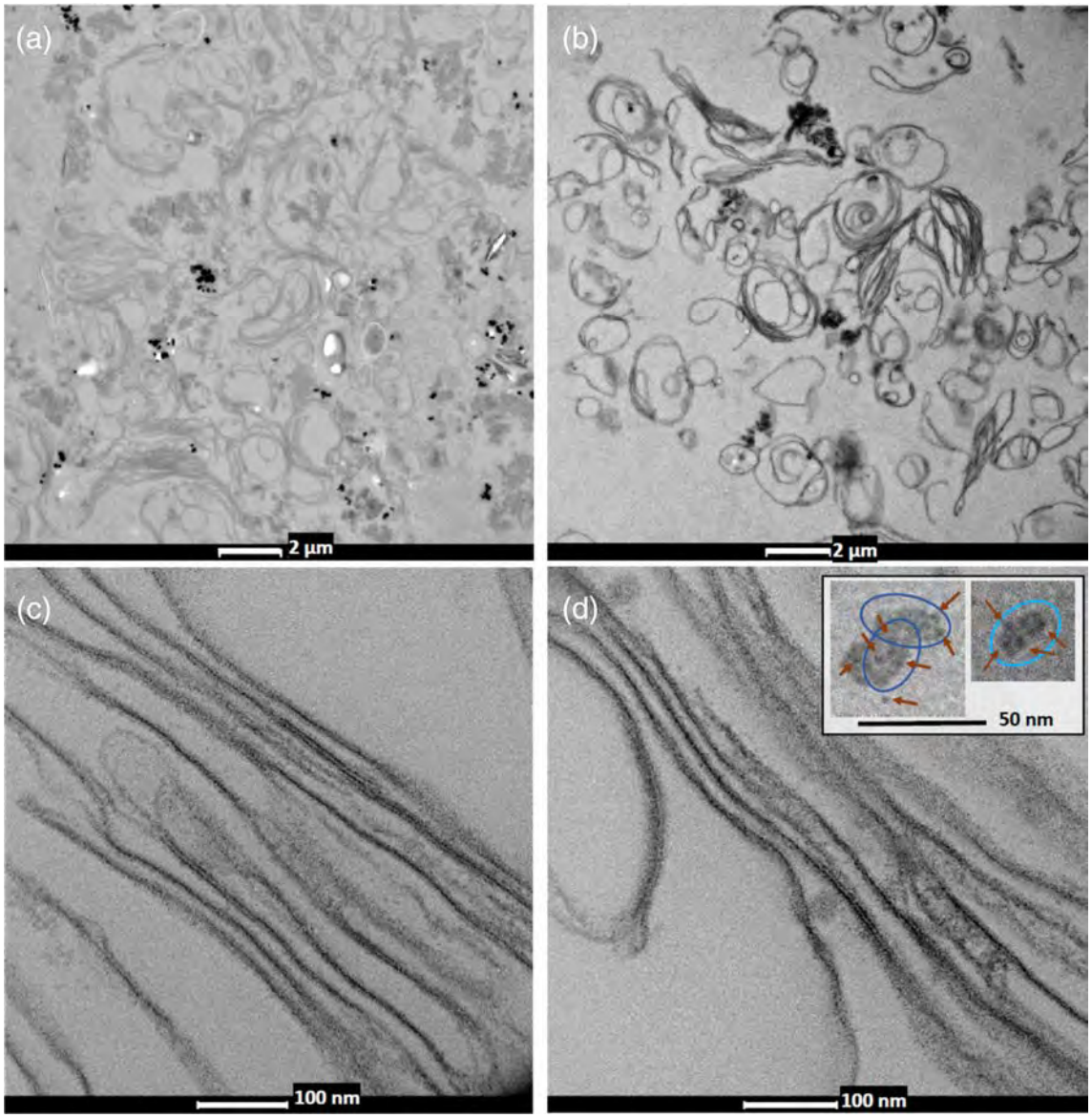

FIGURE 5 Transmission electron microscopy images of BBY PSII: (a) and (c) untreated; (b) and (d) treated with 1 μg NPs/μg Chl. In the inset of figure (d), the structures of PSII complexes with bound LHCII antennas ($C_2S_2M_2$, surrounded by a dark blue frame, the right image) and PSII dimer (C_2, surrounded by a light blue frame, the left image) are shown. Some of the visible superfine WO_3 NPs embedded in these structures are indicated by red arrows.

core) and between 668 and 700 nm (PSII inner antennas: CP43 and CP47), and at ~654 nm (CP43), and (iii) a possible small contribution of Chl *a* from the PSI complex (in this case it is a possible minor contaminant) at around 690 to 705 nm (Alfonso et al., 1994; Bassi et al., 1990; Groot et al., 1995; Groot et al., 1999; Jennings et al., 1990; Konermann & Holzwarth, 1996; Pan et al., 2017). To estimate the position of the bands of different dyes, data obtained for low-temperature spectra with higher resolution can be used because in the 650–690 nm wavelength range, the bands with energies <~14,760 cm^{-1} (λ > ~677 nm) are blue-shifted, and at energies >~ (λ < ~677 nm) the higher energy components are red-shifted by no more than ~1 nm. Only the half-widths Δλ½ of the individual bands increase with increasing temperature from cryogenic to room temperature (up to 40%) (Konermann & Holzwarth, 1996). We can directly compare the spectra because all samples contained the same amount of Chl. From the differential spectra between NP-containing samples and control shown in Figure 6b, it can be seen that for the two lowest concentrations of WO_3 NPs, the contribution of LHCII pigments (chlorophylls *a* and *b* and carotenoids) in absorption spectra decreases (Bressan et al., 2016; Croce et al., 1999). This is most likely due to the appearance of LHCII trimer aggregates in these samples. For isolated LHCII systems, only small changes in absorbance were observed between the isolated LHCII monomers and trimmers and the LHCII aggregates they formed (Lingvay et al., 2020; Magdaong et al., 2013). However, the appearance of a fraction of aggregated LHCII trimmers in reconstituted membranes significantly reduced the intensity of their absorption spectrum over the entire wavelength range for the Soret and QY bands (Lingvay et al., 2020). Therefore, even a small increase in the fraction of LHCII aggregates in PSII BBY treated with 0.0001 and 0.001 μg NP/μg Chl compared to the control sample could have caused the observed changes in the absorption spectra. An increase in absorbance is observed for the 0.01 and 0.1 μg NP/μg Chl weight ratios. In the first case, the shape of the differential spectrum is characteristic of PSII super-complexes with a few LHCII trimmers attached to them (Caffarri et al., 2009) and probably LHCII, as indicated by the absorption maximum at ~523 nm (Ruban et al., 1992). It seems that the higher concentration of m-WO_3 NPs resulted in an increased absorption only in the PSII RC since the peaks at 674, 442, and 419 nm were shifted to 677, 438, and 418 nm, respectively (Seibert et al., 1988). In this case, however, the effect of the increased absorption is less pronounced. For a sample containing 1 μg NP/μg Chl, an inverse trend of the changes in absorbance is observed when the absorbance decreases again in comparison to the control. The shape of the differential spectrum indicates a decrease in the absorption efficiency of the entire PSII-LHCII supercomplex (Eshaghi et al., 1999).

Steady-state fluorescence measurements were performed to investigate the influence of m-WO_3 NPs on the energy transfer efficiency of PSII BBY. Figure 7a–f show room temperature excitation-emission spectra of all samples. To obtain information on the energy transfer from LHCII and the minor antenna to PSII RC for each sample, the fluorescence spectrum obtained by excitation at 440 nm (when equal excitation of Chl *a* and Chl *b* is expected) was subtracted from the fluorescence spectrum excited at a wavelength specific for Chl *b*, that is, 480 nm (Kim et al., 2017; Mackinney, 1941). In each case, the emission spectra were previously normalized to a wavelength of 720 nm. At this wavelength, the fluorescence Chl *a* form PSI dominates, so it is assumed that there is no contribution from PSII fluorescence. These differential spectra for untreated and NP-treated PSII BBYs are shown in Figure 7g. These data provide information on light harvesting and energy transfer from the outer to the inner antenna and PSII core chlorophylls. Thus, the differential spectra show bands from systems capable of absorbing energy from the LHCII complexes and involved in transporting energy to the PSII RC, as well as bands from different LHCII states that are unable to transfer the absorbed energy. The differential spectra obtained for the control and NP-containing samples are clearly different and depend on the concentration of WO_3 NPs. In the control sample, there are some characteristic bands with maxima at about 657.5, 662.5, 677, 684, 690, 700 and 715 nm (black line in Figure 7g). The two bands at the shortest wavelength are most likely related to Chl *b*, which could be observed in quenched PSII complexes, aggregated LHCII, and when Chls *b* are uncoupled in the light-harvesting antenna (Horton et al., 1991; Santabarbara et al., 2001). Bands with maximum emission at about 677–680 nm are from Chl *a*, mainly from monomeric/isolated LHCII trimmers (Standfuss & Kühlbrandt, 2004), while at 700–715 nm from LHCII aggregates (Horton et al., 1991; Yamamoto et al., 2014). In the wavelength range of 680–700 nm, Chls *a* of the inner antenna emit radiation, but CP47 has a larger contribution in the emission at λ ≥ 690 nm, while CP43 has its maximum at ~683–685 nm (Alfonso et al., 1994; Andrizhiyevskaya et al., 2004; Andrizhiyevskaya et al., 2005; Dang et al., 2008; Shibata et al., 2013).

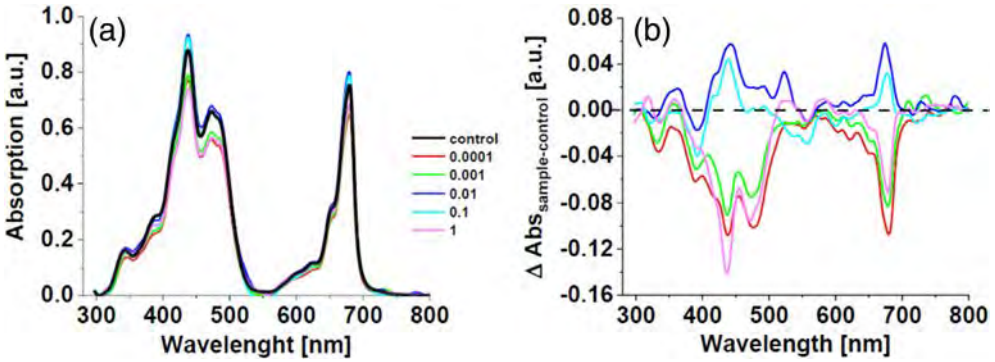

FIGURE 6 (a) Absorption spectra of the control sample and PSII BBY treated with different concentrations of m-WO_3 NPs indicated in the figure. The samples were suspended in the Hepes I buffer, pH 6.5. (b) Differential absorption spectra between samples containing different concentrations of NPs and the control sample.

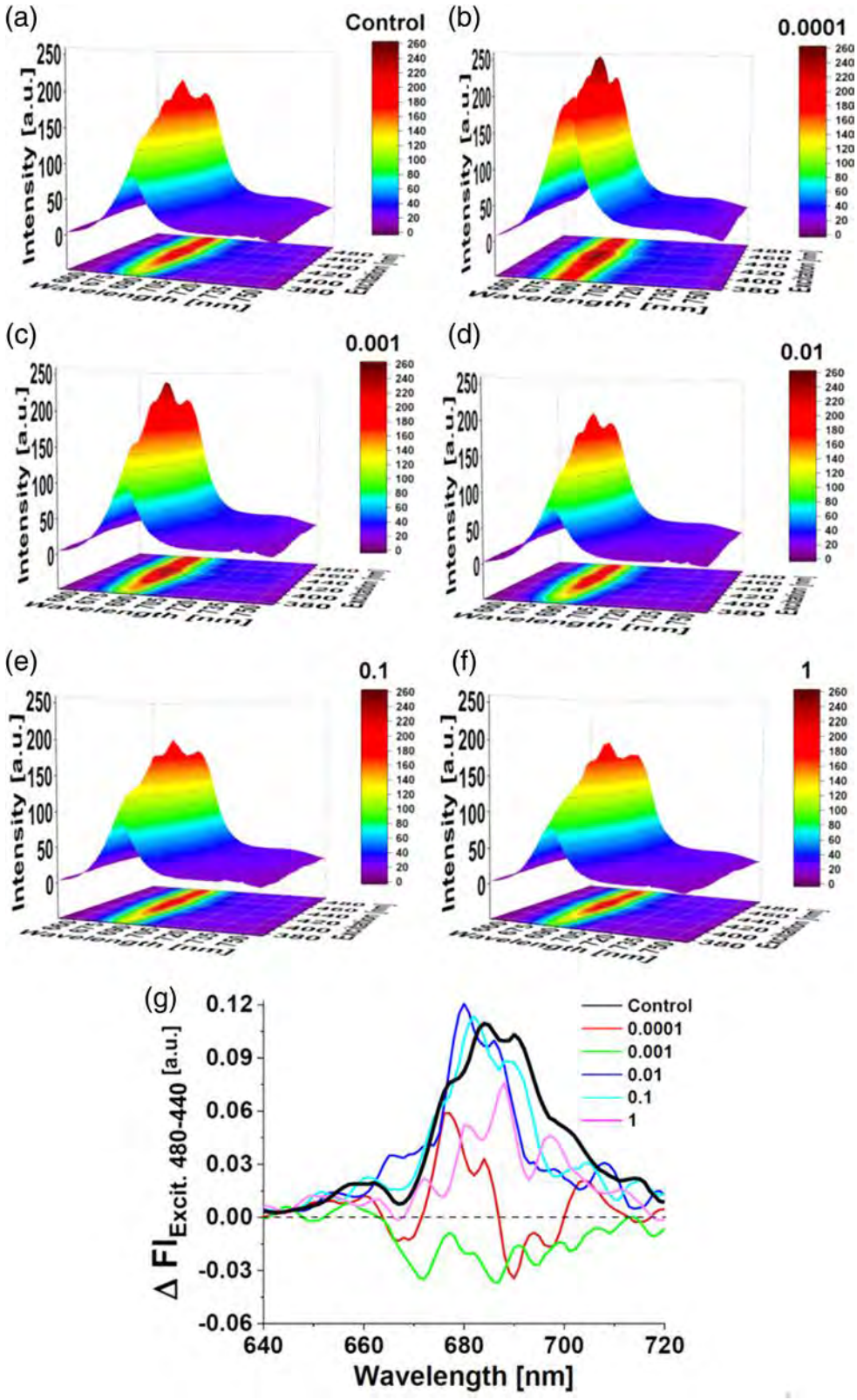

FIGURE 7 Room temperature excitation-emission spectra for a control sample of PSII BBY and treated with different concentrations of m-WO_3 NPs as indicated in the figures (a–f). (g) Differential fluorescence emission spectra at 440 nm excitation (when equal excitation of Chl *a* and Chl *b* is expected) and at 480 nm (Chl *b* excitation) obtained for the control and PSII BBY treated with different concentrations of NPs. The samples were suspended in the Hepes I buffer, pH 6.5.

A fluorescence maximum that is usually observed at 693–695 nm is related to the fluorescence of the lowest excited state of CP47, most likely Chl 612 (Hall et al., 2016). PSII core chlorophylls are expected to show fluorescence between 682 and 687 nm (Chen et al., 2015). Therefore, it is likely that the emission of Chls coupled to the PSII core and CP43 contributes to the band with a maximum at 684 nm, while the band with a maximum at 690 nm is dominated by the emission from the CP47 antenna. Therefore, it can be concluded that in

the control sample the LHCII is effectively transferring energy to the PSII reaction center and that there is good connectivity between the internal and external antennas, as well as with the PSII core. It turned out that even the lowest concentration of 0.0001 μg NP/μg Chl (red line in Figure 7g) caused a disruption of the energy transfer from LHCII to CP47 and from the PSII core to CP47 (which occurs when the reaction centers are closed), since the fluorescence at 684 nm decreased and, decreased in the whole range from 686 to 700 nm. In addition, there are two minima at these wavelengths, at 690 and 697 nm, characteristic of CP47. Therefore, in this sample, CP43 is responsible for the transfer of energy to Chls of the PSII core. There are also two bands with maxima at about 677 and 704 nm. These bands may indicate monomers and aggregates of the LHCII trimmers, respectively. Such states of LHCII are not able to transfer energy to PSII and they emit fluorescence (Lingvay et al., 2020). LHCII fluorescence spectra with characteristic maxima in the range of 670 to 705 nm are due to exciton-phonon coupling. The properties of the lower excited states are determined by localized states of excitons within a small group of Chls in LHCII promoted by static disorder resulting from slower collective motions of proteins at dye binding sites than the characteristic fluorescence lifetime. Lower energy states of LHCII aggregates (λ > 705 nm) are possible in certain conformational states when mixing of an excitonic state with a charge-transfer state occurs (Krüger et al., 2010). A ten-fold higher concentration of NPs leads to an attenuation of the fluorescence over almost the whole range (green line in Figure 7g), indicating a disturbance of the energy transfer between LHCII and the two internal antennas, CP43 and CP47, in some PSII supercomplexes. For the concentration of 0.01 μg NP/μg Chl (dark blue line in Figure 7g), the occurrence of positive bands at 680 and 686 nm, which can be attributed to LHCII and PSII core/CP43, respectively, as well as a band at 708 nm, which indicates antennas aggregation was observed. The broad band at around 665–670 nm may come from decoupled Chls and/or aggregated Chls *b* as well as from minor complex antennas. This differential spectrum indicates the presence of some LHCII aggregates, but also an increase in absorption by LHCII in PSII-LHCII complexes and efficient energy transfer to Chls of the PSII core involving CP43. However, the energy transfer between the Chls coupled to the PSII core and CP43 is reduced in comparison to the control sample, but it is more efficient than in the sample treated with 0.0001 μg NP/μg Chl. The differential fluorescence spectrum of the sample treated with a concentration of 0.1 μg NP/μg Chl (light blue line in Figure 7g) showed positive maxima at about 682 and 689 nm, indicating effective energy transfer within PSII-LHCII complexes from LHCII to both internal antennas, that is, CP43 and CP47, respectively, and their good connectivity to PSII core Chls. The bands with maxima at about 660.6 and 674.4 nm are most likely derived from decoupled Chl *b* and Chl *a* within the LHCII. The two small bands at about 705 and 715 nm are associated with LHCII aggregates. The highest concentration applied (magenta line in Figure 7g) results in an increased fluorescence at about 680.5, 688 and 697 nm. The first band is from monomeric LCHII, while the other two are from CP47. The band at about 712 nm is probably related to some LHCII aggregates. The maximum band at 672 nm comes from decoupled Chls *a*, and these two bands at 651.5 and 660.5 nm are from decoupled Chls *b*. The data indicates that in this case in the PSII-LHCII complex the transfer of energy from the LHCII to the CP43 is disrupted but that LHCII is able to transfer energy to CP47.

4 | DISCUSSION

Photosynthetic membranes are complex biological membranes enriched in proteins and pigments. Their macro-organization depends on environmental stimuli, so thylakoids are dynamic structures (Anderson et al., 2012; Dekker & Boekema, 2005). Their optimal architecture is determined by PSII supercomplexes, which can vary in size depending on the number of LHCII trimers attached. The largest supercomplex contains strongly- and moderately-bound LHCII trimmers ($C_2S_2M_2$, Figure 8), and the minimal unit (C_2S_2) is separated from the two moderately-bound LHCII trimmers (2 M). Still, intermediate states ($C_2S_2M_1$, $C_2S_1M_1$, C_2M_1) and much smaller ones (C_2S_1, C_2M_1, C_2, C_1S_1) are possible (Caffarri et al., 2009), as well as larger supercomplexes (Pagliano et al., 2013). The transformation between these different forms of PSII supercomplexes and their temporal and spatial stabilization under specific conditions, depending on internal and external factors, aims to regulate and optimize the harvest and utilization of light, to facilitate diffusion processes inside and outside the membrane and to keep diffusion times short supporting the repair of light-damaged PSII (reviews: [Kirchhoff, 2008; Mullineaux, 2005]). At the same time, LHCII aggregates may form (Johnson et al., 2011), and the reorganization of PSII core dimers can occur, even leading to PSII

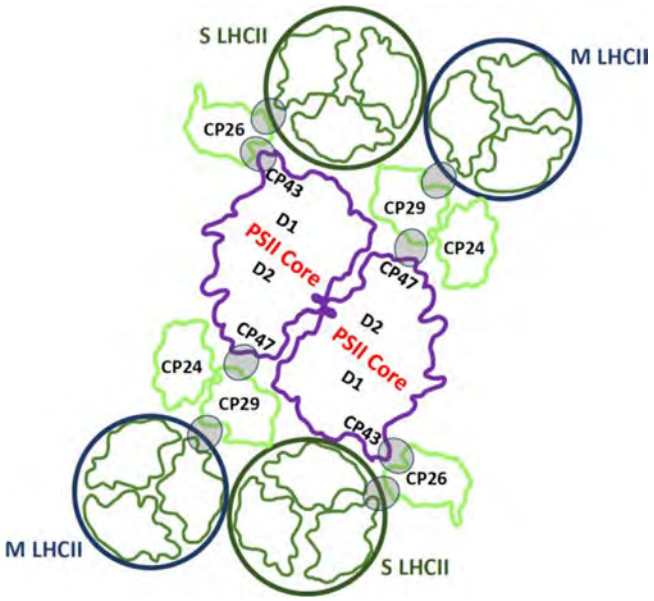

FIGURE 8 Large PSII supercomplex with strongly – (S) and moderately-bound (M) LHCII trimer (C2S2M2). Scheme prepared on the basis of Dekker and Boekema (2005) and Lee et al. (2015). The energy transfer from the external to the internal antennas, which is influenced by very fine m-WO_3 NPs, is marked by gray circles.

monomerization (Caffarri et al., 2009). Dissociation of the PSII supercomplex $C_2S_2M_2$ is one of the photoprotective mechanisms essential for triggering non-photochemical fluorescence quenching (NPQ) (Betterle et al., 2009). A major challenge is to experimentally follow the different mechanisms that control the self-assembly of PSII-LHCII supercomplexes. In this case, the modelling approach has proven to be very helpful. Using a coarse-grained model of thylakoids, including two LHCII trimers (S2) strongly-bound to the PSII core on antenna complexes CP26 and CP43 and two LHCII trimers (2 M) moderately-bound to the PSII core on antenna complexes CP24 and CP29, it was reported that there is a correlation between the free LHC:PSII ratios, the membrane protein packing fraction, and the transitions between the ordered and disordered PSII supercomplex structures. It has been shown that the shifts of the equilibrium states between the individual superstructures $C_2S_2 + 2\ M \leftrightarrow C_2S_2M_1 + M \leftrightarrow C_2S_2M_2$ are reversible and that the long-range order depends on the fluidity of the membrane, and thus, in particular on temperature (Lee et al., 2015).

In addition, different conformers may occur within the supercomplexes. For example, it has been shown that in eukaryotic PSII, a monomeric CP29 antenna can switch between two different C_2S_2 conformations, stretched C_2S_2str and compact C_2S_2comp, by changing its orientation, each of which may exhibit additional structural heterogeneity (Caspy et al., 2021). This flexibility of the PSII dimer core most likely ensures its optimal functioning under global as well as local variable conditions, including (i) efficient utilization of light for charge separation, (ii) access of water and plastoquinones to the donor and acceptor PSII sides, respectively, and (iii) discharge of O_2 and H^+ outside the OEC.

Our BBY PSII membranes contain almost exclusively PSII supercomplexes, as confirmed by the AFM measurements, absorption and fluorescence experiments. Analysis of the distance between the protrusions corresponding to the external OEC protective proteins (Figure 4) observed in the AFM images of BBY PSII in their native liquid environment revealed structural changes in the PSII supercomplexes caused by the presence of superfine m-WO_3 NPs embedded in the membranes. The mean distance between protrusions decreased in PSII BBY treated with 0.0001 μg NPs/μg Chl (∼6.3 nm) compared to the control sample (∼7.1 nm). Moreover, the PSII distribution obtained shows the greatest asymmetry with a simultaneous decrease of the standard deviation at the two lowest NPs concentrations tested. However, the highest density of packing was observed at the concentration of 0.001 μg NPs/μg Chl (distance ∼4.8 nm), for which the standard deviation is the smallest, but the asymmetry of the distribution is large (Figure 4, Table 1). With further increases of NPs concentrations, the separation between PSII cores increases. The standard deviation of the PSII distribution also increases and changes towards a Gaussian distribution as the asymmetry parameter decreases. All the above-described changes in the organization of PSII BBY under the influence of superfine m-WO_3 NPs show that they strongly depend on the concentration of these nanoparticles. The observed differences in the distribution of PSII in supercomplexes are related to compositional and structural changes occurring within them. They can therefore be expected to affect the efficiency of energy capture and transfer from external antennas to internal antennas and the PSII reaction center. Indeed, absorption and fluorescence measurements showed differences between the control sample and PSII BBY treated with NPs. For the two lowest concentrations of NPs a reduced contribution of chlorophylls *a* and *b* from LHCII (Bressan et al., 2016; Croce et al., 1999) in the absorption spectra was observed. At a concentration of 0.0001 μg NPs/μg Chl, this was accompanied by an attenuation of the energy transfer from LHCII to CP47 and formation of LHCII aggregates. At concentration of 0.001 μg NPs/μg Chl, energy transfer between LHCII and the CP43 internal antenna in the PSII supercomplexes was additionally impaired. At the same time, monomerization and aggregation of LCHII trimers was further observed. The direction of these changes is consistent with the knowledge of how the disassembly of large PSII supercomplexes ($C_2S_2M_2$) and the formation of smaller ones affect the energy transfer capabilities of its outer antenna complexes to the inner ones (Barera et al., 2012; Caffarri et al., 2009; Caspy et al., 2021; Su et al., 2017; Wei et al., 2016). In samples treated with higher concentrations of 0.01 and 0.1 μg NPs/μg Chl, the absorbance unexpectedly increased compared to the control. In the first case, the differential spectrum was characteristic of PSII supercomplexes lacking part of the LHCII trimer and the appearance of LHCII aggregates (Caffarri et al., 2009; Ruban et al., 1992). This is consistent with the observation of decoupling the LHCII trimmers from CP47 and the appearance of antenna aggregates, disconnected Chls and disconnected minor antennas, and finally aggregated Chls *b* as deduced from the analysis of fluorescence spectrum. However, the energy flow within PSII-LHCII complexes from LHCII to PSII RC involving CP43 was still efficient. At 10-fold higher concentrations, energy uptake by PSII core dimers increased. This was accompanied by an increase in the efficiency of energy transfer from LHCII to both CP43 and CP47. Other changes regarding the appearance of disconnected Chl *b*/*a* and the aggregation of LHCII and Chls observed at the lower NPs concentration also occur here and are intensified at the highest NPs concentration tested. At a concentration of 1 μg NPs/μg Chl, the decrease in absorption was due to a decrease in the absorption efficiency of large PSII-LHCII supercomplexes. In this case, energy transfer from LHCII to CP43 was impaired but still possible to CP47.

The results show that the external antennas of PSII-LHCII supercomplexes, including LHCII, are particularly sensitive to the action of WO_3 NPs. At the two lowest concentrations of NPs, in addition to an increase in the number of released LHCII trimmers and the formation of their aggregates compared to the control sample, an impairment of the energy transfer through the internal antennas to PSII core Chls was observed, mainly through CP47. However, increasing NPs concentration (0.01 and 0.1 μg NPs/μg Chl) restored energy transfer efficiency through CP43 and at the higher concentration also CP47. The highest concentration of NPs impaired energy uptake in whole fractions of PSII-LHCII supercomplexes, but in contrast to lower concentrations of NPs, energy transfer from external antennas to CP47 was active.

5 | CONCLUSIONS

This work provides new insights into the design of nano-biohybrid systems using photosystem II for O_2 production. Commonly studied 2D/3D semiconductor nanostructures require a large active surface showing a highly specific junction with PSII in order to obtain correctly oriented PSII systems with high packing density. This requires, on the one hand, the functionalization of these meso-nano surfaces and, on the other hand, genetic modifications of the PSII itself. Usually, electron mediators are introduced to ensure electron cycling. Nevertheless, the highest rate of oxygen release recorded for these systems, which they achieve in their initial phase of operation, converted per gram of catalyst, that is, PSII supercomplex remains 2–3 orders of magnitude lower than that exhibited by isolated PSII systems under their native conditions (the highest initial activity for the hybrid systems ranged between 2 and 30 mmol O_2 g_{CAT}^{-1} h^{-1} (Kato et al., 2012; Mersch et al., 2015; Müh & Zouni, 2020; Sokol et al., 2018; Tian et al., 2021) while thylakoids enriched in PSII (PSII BBY) usually show an O_2 yield ~1950 mmol O_2 g_{cat}^{-1} h^{-1},[1] (Berthold et al., 1981; Ghanotakis & Yocum, 1986; Ikeuchi et al., 1985). In this work, an approach to constructing hybrid systems self-organized, based on wild natural PSII BBY has been demonstrated. Superfine m-WO_3 NPs (~1÷2 nm) were introduced into PSII BBY, which showed a concentration-dependent effect on the organization of these membranes and PSII functioning related to the energy transfer. This indicates that the superfine WO_3 NPs easily penetrate the thylakoid membrane and interact with its components. The biohybrid system shows stability at pH 6.5, the native operating environment of PSII, so a high rate of O_2 evolution can be expected. In addition, the light-induced water splitting process can be further stimulated by the direct interaction of superfine WO_3 NPs with the donor and acceptor sides of PSII. The size of PSII of about 10.5 nm in depth, 20.5 nm in length, and 11.0 nm in width (Umena et al., 2011) provides enough space for such small NPs to build in between the structures of this photosystem. It is believed that this approach can facilitate the design of biohybrid systems that convert solar energy into fuel. It allows the use of the entire spectrum of wavelengths emitted by the sun in the UV–VIS range. The activity in water splitting and colloidal system's stability is under investigation.

AUTHOR CONTRIBUTIONS

S. Krysiak: Investigation; writing – original draft; methodology; validation; visualization; formal analysis. **M. Gotić:** Investigation; validation; methodology. **E. Madej:** Investigation; validation; formal analysis; methodology. **A. C. Moreno Maldonado:** Investigation; methodology; validation. **G. F. Goya:** Investigation; methodology; validation. **N. Spiridis:** Investigation; validation; formal analysis; methodology. **K. Burda:** Conceptualization; investigation; writing – original draft; methodology; validation; visualization; formal analysis; supervision.

ACKNOWLEDGMENTS

Sonia Krysiak has been partly supported by the EU Project POWR.03.02.00-00-I004/16. This study was performed within the BIONAN project. We thank Piotr Warszyński for his help with the DLS measurements.

CONFLICT OF INTEREST STATEMENT

The authors declare no conflicts of interest.

DATA AVAILABILITY STATEMENT

The data that support the findings of this study are available from the corresponding author upon reasonable request.

ORCID

K. Burda https://orcid.org/0000-0001-5049-6217

REFERENCES

Alfonso, M., Montoya, G., Cases, R., Rodriguez, R., & Picorel, R. (1994). Core antenna complexes, CP43 and CP47, of higher plant Photosystem II. Spectral properties, pigment stoichiometry, and amino acid composition. *Biochemistry*, *33*, 10494–10500. https://doi.org/10.1021/bi00200a034

Anderson, J. M., Horton, P., Kim, E.-H., & Chow, W. S. (2012). Towards elucidation of dynamic structural changes of plant thylakoid architecture. *Philosophical Transactions of the Royal Society B*, *367*, 3515–3524. https://doi.org/10.1098/rstb.2012.0373

Andrizhiyevskaya, E. G., Chojnicka, A., Bautista, J. A., Diner, B. A., van Grondelle, R., & Dekker, J. (2005). Origin of the F685 and F695 fluorescence in Photosystem II. *Photosynthesis Research*, *84*, 173–180. https://doi.org/10.1007/s11120-005-0478-7

Andrizhiyevskaya, E. G., Frolov, D., van Grondelle, R., & Dekker, J. P. (2004). On the role of the CP47 core antenna in the energy transfer and trapping dynamics of Photosystem II. *Physical Chemistry Chemical Physics*, *6*, 4810–4819. https://doi.org/10.1039/B411977K

Badura, A., Esper, B., Ataka, K., Grunwald, C., Wöll, C., Kuhlmann, J., Heberle, J., & Rögner, M. (2006). Light-driven water splitting for (bio-) hydrogen production: Photosystem 2 as the central part of a bioelectrochemical device. *Photochemistry and Photobiology*, *82*, 1385–1390. https://doi.org/10.1562/2006-07-14-RC-969

Barera, S., Pagliano, C., Pape, T., Saracco, G., & Barber, J. (2012). Characterization of PSII–LHCII supercomplexes isolated from pea thylakoid membrane by one-step treatment with α- and β-dodecyl-d-maltoside. *Philosophical Transactions of the Royal Society B*, *367*(1608), 3389–3399. https://doi.org/10.1098/rstb.2012.0056

Bassi, R., Riconi, F., & Giacome, G. M. (1990). Chlorophyll binding proteins with antenna function in higher plants and green algae. *Photochemistry and Photobiology*, *52*(6), 1187–1206. https://doi.org/10.1111/j.1751-1097.1990.tb08457.x

Berthold, D. A., Babcock, G. T., & Yocum, C. F. (1981). A highly resolved, oxygen-evolving photosystem II preparation from spinach thylakoid membranes. *FEBS Letters*, *134*(2), 231–234. https://doi.org/10.1016/0014-5793(81)80608-4

Betterle, N., Ballottari, M., Morosinotto, T., Zorzan, S., & Bassi, R. (2009). Light-induced dissociation of an antenna hetero-oligomer is needed for non-photochemical quenching induction. *The Journal of Biological*

[1]We performed a rough estimation of the oxygen evolution rate per gram of RC-CP43-CP47 (PSII + two internal light collecting antennas CP43 and CP47, binding a total of 35 Chls) in thylakoids enriched in PSII (BBY PSII) isolated from higher plants. We assumed that per one BBY PSII reaction center, there are additionally 13 LHCII units (units of the external light-harvesting complex - each unit containing 12 Chls) forming two tetramers and one heptameter and three minor antennas CP29, CP26 and CP24 (three monomers containing 27 Chls in total) (Cinque et al., 2000; Croce & van Amerongen, 2011; Müh & Zouni, 2020; Saito et al., 2006; Schmid, 2008). The mass of protein units forming RC, CP43 and CP47 (in total 17 proteins) was taken from (Ke, 2001).

Chemistry, *284*(22), 15255–15266. https://doi.org/10.1074/jbc.M808625200

Boekema, E. J., Hankamer, B., Bald, D., Kruip, J., Nield, J., Boonstra, A. F., Barber, J., & Rögner, M. (1995). Supramolecular structure of the photosystem II complex from green plants and cyanobacteria. *Proceedings. National Academy of Sciences. United States of America*, *92*(1), 175–179. https://doi.org/10.1073/pnas.92.1.175

Bressan, M., Dall'Osto, L., Bargigia, I., Alcocer, M. J., Viola, D., Cerullo, G., D'Andrea, C., Bassi, R., & Ballottari, M. (2016). LHCII can substitute for LHCI as an antenna for photosystem I but with reduced light-harvesting capacity. *Nature Plants*, *2*, 1–10. https://doi.org/10.1038/NPLANTS.2016.131

Burda, K. (2007). Dynamics of electron transfer in photosystem II. *Cell Biochemistry and Biophysics*, *47*(2), 271–284. https://doi.org/10.1007/s12013-007-0011-z

Caffarri, S., Kouřil, R., Kereïche, S., Boekema, E. J., & Croce, R. (2009). Functional architecture of higher plant photosystem II supercomplexes. *The EMBO Journal*, *28*, 3052–3063. https://doi.org/10.1038/emboj.2009.232

Cai, Z.-X., Li, H.-Y., Yang, X.-N., & Guo, X. (2015). NO sensing by single crystalline WO_3 nanowires. *Sensors and Actuators B: Chemical*, *219*, 346–353. https://doi.org/10.1016/j.snb.2015.05.036

Caspy, I., Fadeeva, M., Mazor, Y., & Nelson, N. (2021). Structure of Dunaliella Photosystem II reveals conformational flexibility of stacked and unstacked supercomplexes. In (2021.11.30 ed., pp. 1–29). biorxiv.

Chen, J., Kell, A., Acharya, K., Kupitz, C., Fromme, P., & Jankowiak, R. (2015). Critical assessment of the emission spectra of various photosystem II core complexes. *Photosynthesis Research*, *124*, 253–265. https://doi.org/10.1007/s11120-015-0128-7

Cinque, G., Croce, R., Holzwarth, A., & Bassi, R. (2000). Energy transfer among CP29 chlorophylls: Calculated forster rates and experimental transient absorption at room temperature. *Biophysical Journal*, *79*, 1706–1717. https://doi.org/10.1016/S0006-3495(00)76423-X

Croce, R., Remelli, R., Varotto, C., Breton, J., & Bassi, R. (1999). The neoxanthin binding site of the major light harvesting complex (LHCII) from higher plants. *FEBS Letters*, *456*, 1–6. https://doi.org/10.1016/s0014-5793(99)00907-2

Croce, R., & van Amerongen, H. (2011). Light-harvesting and structural organization of Photosystem II: From individual complexes to thylakoid membrane. *Journal of Photochemistry and Photobiology. B*, *104*, 142–153. https://doi.org/10.1016/j.jphotobiol.2011.02.015

Dang, N. C., Zazubovich, V., Reppert, M., Neupane, B., Picorel, R., Seibert, M., & Jankowiak, R. (2008). The CP43 proximal antenna complex of higher plant photosystem II revisited: Modeling and hole burning study. I. *The Journal of Physical Chemistry. B*, *112*, 9921–9933. https://doi.org/10.1021/jp801373c

Darwent, J. R., & Mills, A. (1982). Photo-oxidation of water sensitized by WO_3 powder. *Journal of the Chemical Society, Faraday Transactions*, *78*, 359–367. https://doi.org/10.1039/F29827800359

De Causmsecker, S., Douglass, J. S., Fantuzzi, A., & Rutherford, A. W. (2019). Energetics of the exchangeable quinone, QB, in Photosystem II. *PNAS*, *116*(39), 19458–19463. https://doi.org/10.1073/pnas.1910675116

Dekker, J. P., & Boekema, E. J. (2005). Supramolecular organization of thylakoid membrane proteins in green plants. *Biochimica et Biophysica Acta*, *1706*, 12–39. https://doi.org/10.1016/j.bbabio.2004.09.009

Eshaghi, S., Andersson, B., & Barber, J. (1999). Isolation of a highly active PSII-LHCII supercomplex from thylakoid membranes by a direct method. *FEBS Letters*, *446*, 23–26. https://doi.org/10.1016/S0014-5793(99)00149-0

Ferreira, K. N., Iverson, T. M., Maghlaoui, K., Barber, J., & Iwata, S. (2004). Architecture of the photosynthetic oxygen-evolving center. *Science*, *303*(5665), 1831–1838. https://doi.org/10.1126/science.1093087

Ghanotakis, F., & Yocum, C. F. (1986). Characterization of a photosystem II reaction center complex isolated by exposure of PSII membrane to a non-ionic detergent and high concentration of NaCl. *Photosynthesis Research*, *10*, 483–488. https://doi.org/10.1007/BF00118314

Gonçalves Silva, C. C., de Moura Torquato, L. D., de Araújo, B. C., Rojas Mantilla, H. D., Boldrin Zanoni, M. V., & Santesso Garrido, S. (2022). Assessment of WO_3 electrode modified with intact chloroplasts as a novel biohybrid platform for photocurrent improvement. *Bioelectrochemistry*, *147*, 108177. https://doi.org/10.1016/j.bioelechem.2022.108177

Gotic, M., Ivanda, M., Popovic, S., & Music, S. (2000). Synthesis of tungsten trioxide hydrates and their structural properties. *Materials Science and Engineering B*, *77*(2), 193–201. https://doi.org/10.1016/S0921-5107(00)00488-8

Grätzel, M. (2001). Photoelectrochemical cells. *Nature*, *414*, 338–344. https://doi.org/10.1142/9789814317665_0003

Grimme, R. A., Lubner, C. E., Bryant, D. A., & Golbeck, J. H. (2008). Photosystem I/molecular wire/metal nanoparticle bioconjugates for the photocatalytic production of H_2. *Journal of the American Chemical Society*, *130*, 6308–6309. https://doi.org/10.1021/ja800923y

Groot, M. L., Frese, R. N., de Weerd, F. L., Bromek, K., Pettersson, Å., Peterman, E. J., van Stokkum, I. H., van Grondelle, R., & Dekker, J. P. (1999). Spectroscopic properties of the CP43 core antenna protein of photosystem II. *Biophysical Journal*, *77*, 3328–3340. https://doi.org/10.1016/S0006-3495(99)77164-X

Groot, M.-L., Peterman, E. J. G., van Stokkum, I. H. M., Dekker, J. P., & van Grondelle, R. (1995). Triplet and fluorescing states of the CP47 antenna complex of photosystem II studied as a function of temperature. *Biophysical Journal*, *68*, 281–290. https://doi.org/10.1016/S0006-3495(95)80186-4

Gust, D., Moore, T. A., & Moore, A. L. (2009). Solar fuels via artificial photosynthesis. *Accounts of Chemical Research*, *42*(12), 1890–1898. https://doi.org/10.1021/ar900209b

Hall, J., Renger, T., Müh, F., Picorel, R., & Krausz, E. (2016). The lowest-energy chlorophyll of photosystem II is adjacent to the peripheral antenna: Emitting states of CP47 assigned via circularly polarized luminescence. *Biochimica et Biophysica Acta*, *1857*, 1580–1593. https://doi.org/10.1016/j.bbabio.2016.06.007

Haniewicz, P., Floris, D., Farci, D., Kirkpatrick, J., Loi, M. C., Büchel, C., Bochtler, M., & Piano, D. (2015). Isolation of plant photosystem II complexes by fractional solubilization. *Frontiers in Plant Science*, *6*, 1100. https://doi.org/10.3389/fpls.2015.01100

Hardee, K. L., & Bard, A. J. (1977). Semiconductor electrodes: X. photoelectrochemical behavior of several polycrystalline metal oxide electrodes in aqueous solutions. *Journal of the Electrochemical Society*, *124*, 215–224. https://doi.org/10.1149/1.2133269

Horton, P., Ruban, A. V., Rees, D., Pascal, A. A., Noctor, G., & Young, A. J. (1991). Control of the light-harvesting function of chloroplast membranes by aggregation of the LHCII chlorophyll-protein complex. *The FEBS Journal*, *292*(1,2), 1–4. https://doi.org/10.1016/0014-5793(91)80819-o

Huang, Z.-F., Song, J., Pan, L., Zhang, X., Wang, L., & Zou, J.-J. (2015). Tungsten oxides for photocatalysis, electrochemistry, and phototherapy. *Advanced Materials*, *27*(36), 5309–5327. https://doi.org/10.1002/adma.201501217

Ihara, M., Nishihara, H., Yoon, K. S., Lenz, O., Friedrich, B., Nakamoto, H., Kojima, K., Honma, D., Kamachi, T., & Okura, I. (2006). Light-driven hydrogen production by a hybrid complex of a [NiFe]-hydrogenase and the cyanobacterial photosystem I. *Photochemistry and Photobiology*, *82*, 676–682. https://doi.org/10.1562/2006-01-16-RA-778

Ikeuchi, M., Yuasa, M., & Inoue, Y. (1985). Simple and discrete isolation of an O_2-evolving PS II reaction center complex retaining Mn and the extrinsic 33 kDa protein. *FEBS Letters*, *185*(2), 316–322. https://doi.org/10.1016/0014-5793(85)80930-3

Ishikita, H., & Knapp, E.-W. (2006). Function of redox-active tyrosine in photosystem II. *Biophysical Journal*, *90*(11), 3886–3896. https://doi.org/10.1529/biophysj.105.076984

Iwuchukwu, I. J., Vaughn, M., Myers, N., O'Neill, H., Frymier, P., & Bruce, B. D. (2010). Self-organized photosynthetic nanoparticle for cell-free hydrogen production. *Nature Nanotechnology*, *5*, 73–79. https://doi.org/10.1038/NNANO.2009.315

Jafari, T., Moharreri, E., Amin, A. S., Miao, R., Song, W., & Suib, S. L. (2016). Photocatalytic water splitting – The untamed dream: A review of recent advances. *Molecules*, *21*, 1–29. https://doi.org/10.3390/molecules21070900

Jennings, R. C., Zucchelli, G., & Garlaschi, F. M. (1990). Excitation energy transfer from the chlorophyll spectral forms to Photosystem II reaction centres: A fluorescence induction study. *Biochimica et Biophysica Acta*, *1016*(2), 259–265. https://doi.org/10.1016/0005-2728(90)90067-E

Johnson, M. P., Goral, T. K., Duffy, C. D. P., Brain, A. P. R., Mullineaux, C. W., & Ruban, A. V. (2011). Photoprotective energy dissipation involves the reorganization of photosystem II light-harvesting complexes in the grana membranes of spinach chloroplasts. *Plant Cell*, *23*, 1468–1479. https://doi.org/10.1105/tpc.110.081646

Joliot, P., Barbieri, G., & Chabaud, R. (1969). Un nouveau modele des centres photochimiques du systeme II. *Photochemistry and Photobiology*, *10*, 309–329. https://doi.org/10.1111/j.1751-1097.1969.tb05696.x

Juelsholt, M., Anker, A. S., Christiansen, T. L., Jørgensen, M. R. V., Kantor, I., Sørensen, D. R., & Jensen, K. M. Ø. (2021). Size-induced amorphous structure in tungsten oxide nanoparticles. *Nanoscale*, *13*(47), 20144–20156. https://doi.org/10.1039/D1NR05991B

Kato, M., Cardona, T., Rutherford, A. W., & Reisner, E. (2012). Photoelectrochemical water oxidation with photosystem II integrated in a mesoporous indium−tin oxide electrode. *Journal of the American Chemical Society*, *134*, 8332–8335. https://doi.org/10.1021/ja301488d

Kato, M., Cardona, T., Rutherford, A. W., & Reisner, E. (2013). Covalent immobilization of oriented photosystem II on a nanostructured electrode for solar water oxidation. *Journal of the American Chemical Society*, *135*(29), 10610–10613. https://doi.org/10.1021/ja404699h

Kato, Y., Sugiura, M., Oda, A., & Watanabe, T. (2009). Spectroelectrochemical determination of the redox potential of pheophytin a, the primary electron acceptor in photosystem II. *Proceedings. National Academy of Sciences. United States of America*, *106*(41), 17365–17370. https://doi.org/10.1073/pnas.0905388106

Kawahara, K., Inoue-Kahino, N., Namie, K., Kato, Y., Tomo, T., Shibata, Y., Kashino, Y., & Noguchi, T. (2020). A gold nanoparticle conjugate with photosystem I and photosystem II for development of a biohybrid water-splitting photocatalyst. *Biomedical Spectroscopy and Imaging*, *9*(1–2), 73–81. https://doi.org/10.3233/BSI-200200

Ke, B. (2001). *Photosynthesis Photochemistry and Photobioiphysics* (Vol. 10). Kluwer Academic Publishers.

Keereeta, Y., Thongtem, S., & Thongtem, T. (2015). Enhanced photocatalytic degradation of methylene blue by WO_3/$ZnWO_4$ composites synthesized by a combination of microwave-solvothermal method and incipient wetness procedure. *Powder Technology*, *284*, 85–94. https://doi.org/10.1016/j.powtec.2015.06.046

Kern, J., & Renger, G. (2007). Photosystem II: Structure and mechanism of the water: Plastoquinone oxidoreductase. *Photosynthesis Research*, *94*, 183–202. https://doi.org/10.1007/s11120-007-9201-1

Kim, E., Akimoto, S., Tokutsu, R., Yokono, M., & Minagawa, J. (2017). Fluorescence lifetime analyses reveal how the high light-responsive protein LHCSR3 transforms PSII light-harvesting complexes into an energy-dissipative state. *The Journal of Biological Chemistry*, *292*(46), 18951–18960. https://doi.org/10.1074/jbc.M117.805192

Kirchhoff, H. (2008). Molecular crowding and order in photosynthetic membranes. *Trends in Plant Science*, *13*(5), 201–207. https://doi.org/10.1016/j.tplants.2008.03.001

Kok, B., Forbush, B., & McGloin, M. (1970). Cooperation of charges in photosynthetic O_2 evolution-I. A linear four step mechanism. *Photochemistry and Photobiology*, *11*(6), 457–475. https://doi.org/10.1111/j.1751-1097.1970.tb06017.x

Konermann, L., & Holzwarth, A. R. (1996). Analysis of the absorption spectrum of photosystem II reaction centers: Temperature dependence, pigment assignment, and inhomogeneous broadening. *Biochemistry*, *35*, 829–842. https://doi.org/10.1021/bi9513158

Krasnovskii, A. A., & Brin, G. P. (1962). Inorganic models of Hill's reaction. *Dokl. Akad. Nauk SSSR Ser. Khim.*, *147*, 656–659.

Krüger, T. P. J., Novoderezhkin, V. N., Ilioaia, C., & van Grondelle, R. (2010). Fluorescence spectral dynamics of single LHCII trimers. *Biophysical Journal*, *98*(12), 3093–3101. https://doi.org/10.1016/j.bpj.2010.03.028

Lee, B. H., Park, S., Kim, M., Sinha, A. K., Lee, S. C., Jung, E., Chang, W. J., Lee, K. S., Kim, J. H., Cho, S. P., & Kim, H. (2019). Reversible and cooperative photoactivation of single-atom Cu/TiO_2 photocatalysts. *Nature Materials*, *18*, 620–626. https://doi.org/10.1038/s41563-019-0344-1

Lee, C.-K., Pao, C.-W., & Smit, B. (2015). PSII-LHCII supercomplex organizations in photosynthetic membrane by coarse-grained simulation. *The Journal of Physical Chemistry. B*, *119*(10), 3999–4008. https://doi.org/10.1021/jp511277c

Li, J., Feng, X., Fei, J., Cai, P., Huang, J., & Li, J. (2016). Integrating photosystem II into a porous TiO_2 nanotube network toward highly efficient photo-bioelectrochemical cells. *Journal of Materials Chemistry A*, *4*, 12197–12204. https://doi.org/10.1039/C6TA04964H

Li, Y., & Tsang, S. C. E. (2020). Recent progress and strategies for enhancing photocatalytic water splitting. *Materials Today Sustainability*, *9*, 1–10. https://doi.org/10.1016/j.mtsust.2020.100032

Lichtenthaler, H. K., & Buschmann, C. (2001). Chlorophylls and Carotenoids: Measurement and Characterization by UV-VIS Spectroscopy. In Current Protocols in Food Analytical Chemistry.

Lingvay, M., Akhtar, P., Sebők-Nagy, K., Páli, T., & Lambrev, P. H. (2020). Photobleaching of chlorophyll in light-harvesting complex ii increases in lipid environment. *Frontiers in Plant Science*, *11*. https://doi.org/10.3389/fpls.2020.00849

Liu, J., & van Iersel, M. W. (2021). Photosynthetic physiology of blue, green, and red light: Light intensity effects and underlying mechanisms. *Frontiers in Plant Science*, *12*. https://doi.org/10.3389/fpls.2021.619987

Liu, Y., Daye, J., Jenson, D., & Fong, S. (2018). Evaluating the efficiency of a photoelectrochemical electrode constructed with photosystem II-enriched thylakoid membrane fragments. *Bioelectrochemistry*, *124*, 22–27. https://doi.org/10.1016/j.bioelechem.2018.06.007

Loopstra, B. O., & Boldrini, P. (1966). Neutron diffraction investigation of WO_3. *Acta Cryst*, *21*, 158–162. https://doi.org/10.1107/S0365110X66002469

Mackinney, G. (1941). Absorption of light by chlorophyll solutions. *The Journal of Biological Chemistry*, *140*(2), 315–322. https://doi.org/10.1016/S0021-9258(18)51320-X

Madey, T. E., & Yates, J. T., Jr. (1968). Desorption by electron impact: Oxygen adsorbed on Tungsten. *Surface Science*, *11*, 327–351. https://doi.org/10.1016/0039-6028(68)90075-7

Magdaong, N. M., Enriquez, M. M., LaFountain, A. M., Rafka, L., & Frank, H. A. (2013). Effect of protein aggregation on the spectroscopic properties and excited state kinetics of the LHCII pigment–protein complex from green plants. *Photosynthesis Research*, *118*, 259–276. https://doi.org/10.1007/s11120-013-9924-0

Mandal, M., Kawashima, K., Saito, K., & Ishikita, H. (2020). Redox potential of the oxygen-evolving complex in the electron transfer cascade of photosystem II. *Journal of Physical Chemistry Letters*, *11*, 249–255. https://doi.org/10.1021/acs.jpclett.9b02831

McConnell, I., Li, G., & Brudvig, G. W. (2010). Energy conversion in natural and artificial photosynthesis. *Chemistry & Biology*, *17*, 434–447. https://doi.org/10.1016/j.chembiol.2010.05.005

McCree, K. J. (1972). The action spectrum, absorptance and quantum yield of photosynthesis in crop plants. *Agricultural Meteorology*, *9*, 191–216. https://doi.org/10.1016/0002-1571(71)90022-7

Mersch, D., Lee, C.-Y., Zhang, J. Z., Brinkert, K., Fontecilla-Camps, J. C., Rutherford, A. W., & Reisner, E. (2015). Wiring of photosystem II to hydrogenase for photoelectrochemical water splitting. *Journal of the American Chemical Society*, *137*(26), 8541–8549. https://doi.org/10.1021/jacs.5b03737

Miyachi, M., Ikehira, S., Nishiori, D., Yamanoi, Y., Yamada, M., Iwai, M., Tomo, T., Allakhverdiev, S. I., & Nishihara, H. (2017). Photocurrent generation of reconstituted photosystem II on self-assembled gold film. *Langmuir*, *33*(6), 1351–1358. https://doi.org/10.1021/acs.langmuir.6b03499

Müh, F., & Zouni, A. (2020). Structural basis of light-harvesting in the photosystem II core complex. *Protein Science*, *29*, 1090–1119. https://doi.org/10.1002/pro.3841

Mullineaux, C. W. (2005). Function and evolution of grana. *Trends in Plant Science*, *10*(11), 521–525. https://doi.org/10.1016/j.tplants.2005.09.001

Nagakawa, H., Takeuchi, A., Takekuma, Y., Noji, T., Kawakami, K., Kamiya, N., Nango, M., Furukawa, R., & Nagata, M. (2019). Efficient hydrogen production using photosystem I enhanced by artificial light harvesting dye. *Photochemical & Photobiological Sciences*, *18*, 309–313. https://doi.org/10.1039/c8pp00426a

Nield, J., & Barber, J. (2006). Refinement of the structural model for the Photosystem II supercomplex of higher plants. *Biochimica et Biophysica Acta*, *1757*(5–6), 353–361. https://doi.org/10.1016/j.bbabio.2006.03.019

Nield, J., Orlova, E. V., Morris, E. P., Gowen, B., van Heel, M., & Barber, J. (2000). 3D map of the plant photosystem II supercomplex obtained by cryoelectron microscopy and single particle analysis. *Nature Structural Biology*, *7*(1), 44–47. https://doi.org/10.1038/71242

Pagliano, C., Saracco, G., & Barber, J. (2013). Structural, functional and auxiliary proteins of photosystem II. *Photosynthesis Research*, *116*, 167–188. https://doi.org/10.1007/s11120-013-9803-8

Pan, J., Gelzinis, A., Chorošajev, V., Vengris, M., Senlik, S. S., Shen, J. R., Valkunas, L., Abramavicius, D., & Ogilvie, J. P. (2017). Ultrafast energy transfer within the photosystem II core complex. *Physical Chemistry Chemical Physics*, *19*(23), 15356–15367. https://doi.org/10.1039/C7CP01673E

Pang, H., Zhao, G., Liu, G., Zhang, H., Hai, X., Wang, S., Song, H., & Ye, J. (2018). Interfacing photosynthetic membrane protein with mesoporous WO_3 photoelectrode for solar water oxidation. *Small*, *14*(19), 1–10. https://doi.org/10.1002/smll.201800104

Pecoraro, V. L., Baldwin, M. J., Caudle, M. T., Hsieh, W.-Y., & Law, N. A. (1998). A proposal for water oxidation in photosystem II. *Pure and Applied Chemistry*, *70*(4), 925–929. https://doi.org/10.1351/pac199870040925

Riedel, M., Wersig, J., Ruff, A., Schuhmann, W., Zouni, A., & Lisdat, F. (2019). A Z-scheme inspired photobioelectrochemical H_2O/O_2 cell with 1V open-circuit voltage combining photosystem II and PbS quantum dots. *Angewandte Chemie, International Edition*, *131*(3), 811–815. https://doi.org/10.1002/ange.201811172

Ruban, A. V., Rees, D., Pascal, A. A., & Horton, P. (1992). Mechanism of ΔpH-dependent dissipation of absorbed excitation energy by photosynthetic membranes. II. The relationship between LHCII aggregation in vitro and qE in isolated thylakoids. *Biochimica et Biophysica Acta*, *1102*, 39–44. https://doi.org/10.1016/0005-2728(92)90062-7

Rutherford, A. W., Mullet, J. E., & Crofts, A. R. (1981). Measurement of the midpoint potential of the pheophytin acceptor of photosystem II. *FEBS Letters*, *123*, 235–237.

Sager, J. C., Smith, W. O., Edwards, J. L., & Cyr, K. L. (1988). Photosynthetic efficiency and phytochrome photoequilibria determination using spectral data. *Transactions of ASAE*, *31*(6), 1882–1889. https://doi.org/10.13031/2013.30952

Saito, K., Kikuchi, T., Nakayama, M., Mukai, K., & Sumi, H. (2006). A single chlorophyll in each of the core antennas CP43 and CP47 transferring excitation energies to the reaction center in Photosystem II of photosynthesis. *Journal of Photochemistry and Photobiology A*, *178*, 271–280. https://doi.org/10.1016/j.jphotochem.2005.10.038

Santabarbara, S., Neverov, K. V., Garlaschi, F. M., Zucchelli, G., & Jennings, R. C. (2001). Involvement of uncoupled antenna chlorophylls in photoinhibition in thylakoids. *FEBS Letters*, *491*, 109–113. https://doi.org/10.1016/S0014-5793(01)02174-3

Schmid, V. H. R. (2008). Light-harvesting complexes of vascular plants. *Cellular and Molecular Life Sciences*, 65, 3619–3639. https://doi.org/10.1007/s00018-008-8333-6

Seibert, M., Picorel, R., Rubin, A. B., & Connolly, J. S. (1988). Spectral, photophysical, and stability properties of isolated photosystem II reaction center. *Plant Physiology*, *87*, 303–306. https://doi.org/10.1104/pp.87.2.303

Shibamoto, T., Kato, Y., Sugiura, M., & Watanabe, T. (2009). Redox potential of the primary plastoquinone electron acceptor Q(A) in photosystem II from Thermosynechococcus elongatus determined by spectroelectrochemistry. *Biochemistry*, *48*(45), 10682–10684. https://doi.org/10.1021/bi901691j

Shibata, Y., Nishi, S., Kawakami, K., Shen, J.-R., & Renger, T. (2013). Photosystem II does not possess a simple excitation energy funnel: Time-resolved fluorescence spectroscopy meets theory. *Journal of the American Chemical Society*, *135*, 6903–6914. https://doi.org/10.1021/ja312586p

Sokol, K. P., Robinson, W. E., Warnan, J., Kornienko, N., Nowaczyk, M. M., Ruff, A., Zhang, J. Z., & Reisner, E. (2018). Bias-free photoelectrochemical water splitting with photosystem II on a dye-sensitized photoanode wired to hydrogenase. *Nature Energy*, *3*, 944–951. https://doi.org/10.1038/s41560-018-0232-y

Standfuss, J., & Kühlbrandt, W. (2004). The Three Isoforms of the Light-harvesting complex II: Spectroscopic features, trimer formation, and functional roles. *The Journal of Biological Chemistry*, *279*(35), 36884–36891. https://doi.org/10.1074/jbc.M402348200

Stoichev, S., Krumova, S. B., Andreeva, T., Busto, J. V., Todinova, S., Balashev, K., Busheva, M., Goni, F. M., & Taneva, S. G. (2015). Low pH modulates the macroorganization and thermal stability of PSII supercomplexes in grana membranes. *Biophysical Journal*, *108*(4), 844–853. https://doi.org/10.1016/j.bpj.2014.12.042

Su, X., Ma, J., Wei, X., Cao, P., Zhu, D., Chang, W., Liu, Z., Zhang, X., & Li, M. (2017). Structure and assembly mechanism of plant $C_2S_2M_2$-type PSII-LHCII supercomplex. *Science*, *357*(6353), 815–820. https://doi.org/10.1126/science.aan0327

Sumathi, M., Prakasam, A., & Anbarasan, P. M. (2019). High capable visible light driven photocatalytic activity of WO_3/g-C_3N_4 hetrostructure catalysts synthesized by a novel one step microwave irradiation route. *Journal of Materials Science: Materials in Electronics*, *30*, 3294–3304. https://doi.org/10.1007/s10854-018-00602-4

Sznee, K., Dekker, J. P., Dame, R. T., van Roon, H., Wuite, G. J. L., & Frese, R. N. (2011). Jumping mode atomic force microscopy on grana membranes from spinach. *The Journal of Biological Chemistry*, *286*(45), 39164–39171. https://doi.org/10.1074/jbc.M111.284844

Tahara, K., Mohamed, A., Kawahara, K., Nagao, R., Kato, Y., Fukumura, H., Shibata, Y., & Noguchi, T. (2017). Fluorescence property of photosystem II protein complexes bound to a gold nanoparticle. *Faraday Discussions*, *198*, 121–134. https://doi.org/10.1039/C6FD00188B

Tanisaki, S. (1960). Crystal structure of monoclinic tungsten trioxide at room temperature. *Journal of the Physical Society of Japan*, *15*, 573–581. https://doi.org/10.1143/JPSJ.15.573

Terasaki, N., Iwai, M., Yamamoto, N., Hiraga, T., Yamada, S., & Inoue, Y. (2008). Photocurrent generation properties of Histag-photosystem II immobilized on nanostructured gold electrode. *Thin Solid Films*, *516*(9), 2553–2557.

Tian, W., Zhang, H., Sibbons, J., Sun, H., Wang, H., & Wang, S. (2021). Photoelectrochemical water oxidation and longevous photoelectric conversion by a Photosystem II electrode. *Advanced Energy Materials*, *11*(30), 2100911. https://doi.org/10.1002/aenm.202100911

Umena, Y., Kawakami, K., Shen, J.-R., & Kamiya, N. (2011). Crystal structure of oxygen-evolving photosystem II at a resolution of 1.9Å. *Nature*, *473*, 55–61. https://doi.org/10.1038/nature09913

Utschig, L. M., Dimitrijevic, N. M., Poluektov, O. G., Chemerisov, S. C., Mulfort, K. L., & Tiede, D. M. (2011). Photocatalytic hydrogen production from noncovalent biohybrid photosystem I/Pt nanoparticle complexes. *Journal of Physical Chemistry Letters*, *2*, 236–241. https://doi.org/10.1021/jz101728v

Utschig, L. M., Zaluzec, N. J., Malavath, T., Ponomarenko, N. S., & Tiede, D. M. (2023). Solar water splitting Pt-nanoparticle photosystem I thylakoid systems: Catalyst identification, location and oligomeric structure. *Biochimica et Biophysica Acta*, *1864*(3), 148974. https://doi.org/10.1016/j.bbabio.2023.148974

van Bezouwen, L. S., Caffarri, S., Kale, R. S., Kouřil, R., Thunnissen, A.-M. W. H., Oostergetel, G. T., & Boekema, E. J. (2017). Subunit and chlorophyll organization of the plant photosystem II supercomplex. *Nature Plants*, *3*, 17080. https://doi.org/10.1038/nplants.2017.80

Vass, I., & Styring, S. (1991). pH-dependent charge equilibria between tyrosine-D and the S states in photosystem II. Estimation of relative midpoint redox potentials. *Biochemistry*, *30*(3), 830–839. https://doi.org/10.1021/bi00217a037

Vittadello, M., Gorbunov, M. Y., Mastrogiovanni, D. T., Wielunski, L. S., Garfunkel, E. L., Guerrero, F., Kirilovsky, D., Sugiura, M., Rutherford, A. W., Safari, A., & Falkowski, P. G. (2010). Photoelectron generation by photosystem II core complexes tethered to gold surfaces. *ChemSusChem*, *3*, 471–475. https://doi.org/10.1002/cssc.200900255

Voloshin, R. A., Shumilova, S. M., Zadneprovskaya, E. V., Zharmukhamedov, S. K., Alwasel, S., Hou, H. J. M., & Allakhverdiev, S. I. (2022). Photosystem II in bio-photovoltaic devices. *Photosynthetica*, *60*(1), 121–135. https://doi.org/10.32615/ps.2022.010

Wang, W., Wang, Z., Zhu, Q., Han, G., Ding, C., Chen, J., Shen, J. R., & Li, C. (2015). Direct electron transfer from photosystem II to hematite in a hybrid photoelectrochemical cell. *Chemical Communications*, *51*(95), 16952–16955. https://doi.org/10.1039/C5CC06900A

Wang, Y., Chen, D., Hu, Y., Qin, L., Liang, J., Sun, X., & Huang, Y. (2020). An artificially constructed direct Z-scheme heterojunction: WO_3 nanoparticle decorated $ZnIn_2S_4$ for efficient photocatalytic hydrogen production. *Sustainable Energy & Fuels*, *4*, 1681–1692. https://doi.org/10.1039/C9SE01158G

Wasilewski, M. R. (2009). Self-assembly strategies for integrating light harvesting and charge separation in artificial photosynthetic systems. *Accounts of Chemical Research*, *42*(12), 1910–1921. https://doi.org/10.1021/ar9001735

Wei, X., Su, X., Cao, P., Liu, X., Chang, W., Li, M., Zhang, X., & Liu, Z. (2016). Structure of spinach photosystem II–LHCII supercomplex at 3.2 Å resolution. *Nature*, *534*, 69–74. https://doi.org/10.1038/nature18020

Xu, Y., Li, A., Yao, T., Ma, C., Zhang, X., Shah, J. H., & Han, H. (2017). Strategies for efficient charge separation and transfer in artificial photosynthesis of solar fuels. *ChemSusChem*, *10*, 4277–4305. https://doi.org/10.1002/cssc.201701598

Yamamoto, Y., Kai, S., Ohnishi, A., Tsumura, N., Ishikawa, T., Hori, H., Morita, N., & Ishikawa, Y. (2014). Quality control of PSII: Behavior of PSII in the highly crowded grana thylakoids under excessive light. *Plant & Cell Physiology*, *55*(7), 1206–1215. https://doi.org/10.1093/pcp/pcu043

Yamanoi, Y., Nakae, T., & Nishihara, H. (2021). Bio-organic-inorganic hybrid soft materials: Photoelectric conversion systems based on photosystem I and II with molecular wires. *Chemistry Letters*, *50*(6), 1263–1270. https://doi.org/10.1246/cl.210111

Yehezkeli, O., Tel-Vered, R., Wasserman, J., Trifonov, A., Michaeli, D., Nechushtai, R., & Willner, I. (2012). Integrated photosystem II-based photo-bioelectrochemical cells. *Nature Communications*, *3*, 742. https://doi.org/10.1038/ncomms1741

Yehezkeli, O., Willner, I., Tel-Vered, R., Michaeli, D., & Nechushtai, R. (2014). Photosynthetic reaction center-functionalized electrodes for photo-bioelectrochemical cells. *Photosynthesis Research*, *120*, 71–85. https://doi.org/10.1007/s11120-013-9796-3

Zhang, J. Z., & Reisner, E. (2020). Advancing photosystem II photoelectrochemistry for semi-artificial photosynthesis. *Nature Reviews Chemistry*, *4*, 6–21. https://doi.org/10.1038/s41570-019-0149-4

Zhao, J., Wang, X., Xu, Z., & Loo, J. S. C. (2014). Hybrid catalysts for photoelectrochemical reduction of carbon dioxide: A prospective review on semiconductor/metal complex co-catalyst systems. *Journal of Materials Chemistry A*, *2*, 15228–15233. https://doi.org/10.1039/c4ta02250e

How to cite this article: Krysiak, S., Gotić, M., Madej, E., Moreno Maldonado, A. C., Goya, G. F., Spiridis, N., & Burda, K. (2023). The effect of ultrafine WO_3 nanoparticles on the organization of thylakoids enriched in photosystem II and energy transfer in photosystem II complexes. *Microscopy Research and Technique*, 1–16. https://doi.org/10.1002/jemt.24394